# Tracks of 30-MeV C60 clusters in Yttrium Iron Garnet Studied by Scanning Force Microscopy

A. El-Said

# Tracks of 30-MeV $C_{60}$ clusters in Yttrium Iron Garnet Studied by Scanning Force Microscopy

A.S. El-Said

*Nuclear and Radiation Physics Lab., Physics Department, Faculty of Science, Mansoura University, 35516 Mansoura, Egypt.*

Yttrium iron garnet ($Y_3Fe_5O_{12}$ or YIG), an amorphizable ferrimagnetic insulator, is probably the best studied material with respect to track formation and damage morphology. This paper presents first scanning force microscopy (SFM) of surface damage induced by energetic $C_{60}$ clusters. YIG single crystals were irradiated at normal incidence with 30-MeV $C_{60}$ cluster ions (kinetic energy~0.04 MeV/u) provided by the tandem accelerator of the Institute of Nuclear Physics in Orsay (IPNO). The SFM topographic images show nano-protrusions on the YIG surface, where each hillock is generated by one $C_{60}$ cluster. The role of stopping power and deposited energy density is discussed in terms of dimensional analysis of the nanostructures. Hillocks created by $C_{60}$ clusters are compared with those produced by monatomic ions.

*Keywords:* ion tracks, $Y_3Fe_5O_{12}$, clusters, energy loss, SFM.

*PACS:* 61.80.Jh; 68.37.Ps; 79.20.Rf

Corresponding Address

*Nuclear and Radiation Physics Lab., Physics Department, Faculty of Science; Mansoura University, 35516 Mansoura, Egypt*

E-mail address a_s_elsaid@mans.edu.eg

## 1. INTRODUCTION

Track formation in solids using energetic ion particles is of high interest not only due to basic phenomena concerning ion-solid interaction but also due to promising technological applications, especially the synthesis of nanostructures using ion beam based methods [1-5]. Fast heavy ions, passing through material, deposit their energy predominantly by inelastic collisions (electronic energy loss $(dE/dx)_e$). In many materials such electronic excitation and ionizations may finally lead to structural modifications along the trajectories of the projectiles producing so-called ion tracks [6]. The creation mechanism and the morphology of ion tracks were studied in many different materials. In the past, the data set on track size, structure, and (dE/dx) formation threshold has largely increased, in particular for amorphizable materials such as mica [7-10], $SiO_2$ [11] and various spinels [12], as well as for non-amorphizable materials including radiation resist oxides ($UO_2$, $Al_2O_3$) [13-16], and fluoride ionic crystals (e.g. LiF, $CaF_2$, $BaF_2$ $MgF_2$ and $LaF_3$) [17,18]. For this field of research the availability of several heavy ion accelerator facilities (such as GSI, GANIL, and JAERI) producing light ions up to very heavy species (e.g. uranium) in the MeV-GeV energy regime was a key issue. It also should be mentioned that the successful production of MeV cluster ion beam has helped to improve the understanding of ion-matter interaction processes because the stopping power $(dE/dx)_e$ reached with cluster ions even with low Z values (eg. $C_n$, n is number of the constituents of the cluster) is comparable to, and even higher (in case of high n, eg. n = 60), than for GeV monatomic heavy ions. In addition, the density of the electronic energy deposition can reach very high value due to the smaller velocity of the interacting cluster ions. This energy density criterion was originally suggested by Katz [19], an analytical formula for the radial dose deposition was proposed by Waligorski et al. [20]. In later studies, the influence of radial dose or energy density was evidenced and termed velocity effect [21]. It is based on the fact that the volume in which dE/dx is deposited is larger the higher is the ion

velocity. Therefore, given by the low clusters velocity as well as their large energy loss, track creation and the accompanied processes such as sputtering are more efficient in comparison to fast monatomic ions. $C_{60}$ clusters of several MeV are for instance able to induce ion-tracks in a Si target [22], whereas track formation has never been observed when using GeV monatomic heavy ions.

For getting information about the track size and morphology, different techniques including Rutherford backscattering (RBS), small angle x-ray scattering (SAXS), high resolution electron microscopy (HREM, TEM) were applied. Although TEM has the advantage of being able to image ion tracks in the bulk with thickness up to hundred nanometers, the technique is accompanied by difficulties with respect to sample preparation, image contrast, and track stability in the electron beam [23]. Scanning force microscopy (SFM), with its ability for measuring surface nanostructures, overcomes these limitations. In the recent past, SFM has successfully been applied for studying the surface damage induced by both monatomic heavy ions, and MeV $C_{60}$ clusters in $CaF_2$ and $LaF_3$ as examples of non-amorphizable materials [24]. In this study, yttrium iron garnet ($Y_3Fe_5O_{12}$ or YIG) is selected as a target for investigating the role of the electronic energy loss and the density of energy deposition. The selection of this material is motivated by the large data set already existing for tracks created by different ion-beams [25-27]. Also surface structuring of YIG for possible technological application as a magnetic insulating material is of interest [28].

## 2. EXPERIMENT

YIG crystals were grown on 0.5 μm thick $Gd_3Ga_5O_{12}$ substrates and had a thickness of 100 μm thick and size of 25 $mm^2$. The irradiation with 30 MeV $C_{60}$ cluster ions was performed at room temperature, under normal incidence and applying a fluence of approximately $10^{10}$ cluster/$cm^2$. The cluster beam was provided by the 10-MV tandem accelerator of the Institute

of Nuclear Physics in Orsay (IPNO). In the first section of the tandem, negative $C_{60}$ ions are accelerated. At the positive high voltage terminal in the center of the accelerator, the negative $C_{60}$ ions interact with nitrogen molecules in a stripper cell and become multiply positively charged $C_{60}^{q+}$ ( $q \leq 4$) [29]. For this experiment, we used $C_{60}^{2+}$ leading to kinetic energy of 30 MeV. The energy loss values and projected ranges of the incident projectiles were calculated using the SRIM 2006 code [30], assuming that the energy loss for $C_{60}$ clusters corresponds to the sum of the energy loss of the constituent single carbon ions of the same velocity ($v/c \sim 0.01$). The validity of this assumption is confirmed by several experiments [31, 32].

The YIG irradiated surfaces were probed by MFP-3D scanning force microscope (Asylum Research, Santa Barbara, US). This SFM system is placed on a sensitive active anti-vibration stage and equipped with closed-loop nanopositioning system sensors for the correction of piezo hysteresis and creep. The measurements have been performed in contact mode at constant loading force below 10 nN using non-conductive $Si_3N_4$ sensors (Veeco Instruments, France) with cantilevers of force constants of 0.1 N/m. All the measured SFM images were recorded using MFP-3D IGOR Pro software and processed with the Nanotec Electronica SL WSxM software (version 4.0 Develop 9.3).

## 3. RESULTS AND DISCUSIONS

A typical SFM topographic image of YIG surface after irradiation with 30-MeV $C_{60}$ is shown in Fig.1. The image displays hillock-like nanostructures protruding from the surface. The hillocks shape is circular. The number of hillocks per unit area is in good agreement with the applied ion fluence, i.e., each hillock is created by an individual cluster impact. The analysis of the hillock dimensions was performed by recording the diameter and the respective height of each individual hillock using line profiling. It should be mentioned that for the estimation of the diameter of the $C_{60}$-induced hillocks, the foot point method [24] was applied, whereas

in case of monatomic ions, the diameters were estimated as 2.35 FWHM from the Gaussian fitting curve of the hillock line profile [33]. The diameters of the hillocks, produced by $C_{60}$, cover values between 40 and 50 nm, and heights between 5 and 15 nm. The frequency distribution of the hillock parameters are illustrated in Fig. 2. Compared to track diameters deduced from a TEM study [26], the diameters of the hillocks are by almost a factor of two larger. At present, it is not possible to explain this difference because of there are not sufficient data available to clarify if surface hillocks and tracks in the bulk have in general the same diameter. In addition, some of the size difference may origin from the fact that the hillocks could be subjected to a shift of few nanometers due to the finite curvature radius of the used tips (nominally 4-5 nm). It is also noted that the data obtained for the $C_{60}$-irradiated surfaces were recorded with a different SFM tip than the results from samples exposed to monatomic ions. Thus as a matter of consistency, no correction by deconvolution procedure has been included.

Figure 3 illustrates the correlation between the hillock diameter and height. Hillocks with larger diameters exhibit a larger height. The correlation coefficient is given by the formula [33]

$$\rho = \frac{E(DH) - E(D)E(H)}{(Var(D)\,Var(H))^{0.5}} \qquad (1)$$

where E represents the mean values and *Var* denotes the respective variance of the diameter D and height H. For the $C_{60}$ irradiation, $\rho$ is 0.74 close to the correlation coefficient of hillocks produced by monatomic ions which scatters between 0.8 and 0.9 for energy losses between 28 and 41 keV/nm. Such a pronounced correlation between the diameter and the height has already been observed earlier in non-amorphizable materials such as $CaF_2$ and $LaF_3$ [24, 33], and has been interpreted as an indication for continuous track morphology. The absence of a strong dE/dx dependence of the hillock diameter-height correlation can thus be an indication

that the tracks below the sample surface are quasi cylindrical, which would be in agreement with earlier morphology studies exhibiting homogeneous cylinders above ~20 keV/nm. Figure 4 shows the mean diameter and height of hillocks produced by $C_{60}$ clusters and by different monatomic ions [34] as a function of $(dE/dx)_e$. The diameters of the hillocks from monatomic ions scatter around 20 nm, whereas 30 MeV $C_{60}$ clusters induce significantly larger hillocks of mean diameter of 45 nm. In contrast to the size of the hillock diameters, which are possibly affected by the curvature of the used tip, the hillock height exhibits a clear linear dependence on $(dE/dx)_e$. Extrapolating the fit curve gives a $(dE/dx)_e$ threshold of (6.1 ± 0.9) keV/nm, which is in fair agreement with estimations of previous studies, where tracks are observed above 4-5 keV/nm [26, 35].

Earlier high-resolution electron microscopy studies on YIG bombarded with MeV $C_{60}$ clusters, by Dunlop and Jensen, revealed that the tracks produced in the bulk are amorphized zones [26]. With increasing $(dE/dx)_e$, the track morphology evolves from aligned droplets to a continuous cylinder [35]. In addition, it was seen that the track diameters are constant along approximately the first 100 nm below the surface (correlated cluster trajectory), whereas at larger penetration depth, the tracks dissolve because of cluster dissociation. [36]. The parameters of our irradiation, and the experiments we compare our data to, are summarized in Table.1. For monatomic ions as well as for $C_{60}$ clusters, the electronic energy loss is much higher than the nuclear energy loss. It should be noted also that the projected cluster range deduced by the SRIM code does not take into account that the coherence length of the $C_{60}$ clusters is only around 100 nm before the cluster fragments into smaller constituents [37].

As demonstrated in several studies, the size of the tracks does not only depend on $(dE/dx)_e$ but also on the ion velocity, which determines the range of the primary electron cascade and therefore the density of the deposited energy [21]. The velocity of 30-MeV $C_{60}$ clusters is

about one order of magnitude lower than that of monatomic ions (Table 1), thus the effect on hillock formation may be quite pronounced. For a first estimation, the density of the deposited energy was calculated based on energy dissipation according to thermal spike model concept [38]. The radius in which the initial energy is deposited is determined from the radial spread within the electron system and subsequently diffusing into the lattice system. The ion energy transferred to the electrons is assumed to be concentrated within a cylinder radius $R_e$ (corresponding to 66 % of the total electronic energy loss). Via coupling of the electronic and lattice system (with $\lambda$ being the mean electron-phonon interaction mean free path), the energy is finally spread to a radius $R_a = (R^2_e + \lambda^2)^{0.5}$. $R_e$ values for different ion velocities were deduced from Monte Carlo simulations of the radial energy distribution [39]. As $\lambda$ we inserted 5 nm which is a mean value obtained from thermal spike model calculations fitting a large set of experimental track radii [40, 41]. The energy density $\varepsilon$ (eV/atom) deposited in the lattice is then obtained by $\varepsilon = (dE/dx)_e / N \pi R_a^2$, where N is the atomic density of YIG. Due to difficulty to deconvolution of the hillock diameter and the tip size of the SFM, we evaluate only the evolution of the height as a function of $\varepsilon$ (Fig. 5). These data follow a $\varepsilon^{\sim 0.5}$ law and exhibit an energy density threshold of $\varepsilon_{th}$ ~0.7 eV/atom. For YIG, the melting energy is 0.55 eV/atom [42] close to the observed threshold value. It is thus suggested that hillock creation is directly linked to a process where the deposited energy is sufficiently high to melt the material.

**CONCLUSIONS**

In yttrium iron garnet, 30-MeV $C_{60}$ clusters create larger surface hillocks than swift monatomic heavy ions. The electronic energy loss threshold for hillock creation in YIG is (6.1 ± 0.9) keV/nm. The effect of projectile velocity was taken into account by analysing the hillock size as a function of the deposited energy density ranging from 1.7 to 9.6 eV/atom for Ni up to $C_{60}$, respectively. The deposited energy density leads to the creation of hillocks above

a threshold of 0.7 eV/atom, which is close to the energy required for melting. This observation shows the high relevance of thermal spike model for the description of surface hillock formation in YIG.

**ACKNOWLEDGEMENTS**

I wish to express my grateful thanks to C. Trautmann and M. Toulemonde for their valuable comments and suggestions. The support from S. Della-Negra during irradiation of the samples in (IPNO) Orsay is greatly acknowledged. Many thanks to F. Aumayr for giving me the possibility to perform the investigations of the materials in his group at the IAP in Vienna.

**REFERENCES**

[1] J. Krauser, J.-H, Zollondz, A.Weidinger, C. Trautmann, J. Appl. Phys. 94 (2003) 1959.

[2] S. Karim, M.E. Toimil-Molares, A.G. Balogh, W. Ensinger, T.W. Cornelius, E.U. Khan, R. Neumann, NANOTECHNOLOGY 17 (2006) 5954.

[3] R. Spohr, in: Ion Tracks and Microtechnology. Basic Principles and Applications, ed. K. Bethge, Vieweg (1990)

[4] M. Toulemonde, E. Balanzat, S. Bouffard and JC Jousset, Nucl. Instr. Meth. **B 39** (1989)1.

[5] M Skupinski, M. Toulemonde, M. Lindeberg, K. Hjort, Nucl. Instr. Meth. **B 240** (2005)681.

[6] M. Toulemonde, C Trautmann, E Balanzat, K Hjort, A Weidinger Nucl. Instr. Meth. **B 216** (2004) 1.

[7] J. Vetter, R. Scholz, D. Dobrev, L. Nistor, Nucl. Instr. Meth. **B 141** (1998) 747.

[8] F. Thibaudau and J. Cousty, E. Balanzat and S. Bouffard, Phys. Rev. Lett. **76** (1991) 1582.

[9] R. Neumann, Nucl. Instr. Meth. **B 151** (1999) 42.

[10] D. Albrecht, P. Armbruster, R. Spohr, M. Roth, K. Schaupert, H. Stuhrmann, Appl. Phys. **A 37** (1985) 37.

[11] M. Toulemonde, E. Balanzat, S. Bouffard, J.J. Grob, M. Hage-Ali, J.p. Stoquert Nucl. Instr. Meth. **B 46** (1990) 64.

[12] F. Studer, H Pascard, D. Groult, C. Houpert, N. Nguyen, M. Toulemonde, Nucl. Instr. Meth. **B 32** (1988) 389.

[13] Hj. Matzke, P.G. Lucuta, T. Wiss, Nucl. Instr. Meth. **B 166-167** (2000) 920.

[14] T. Wiss, Hj. Matzke, C. Trautmann, M. Toulemonde, S. Klaumünzer, Nucl. Instr. Meth. **B 122** (1997) 583.

[15] B. Canut, A. Benyagoub, G. Marest, A. Meftah, N. Moncoffre, S.M.M. Ramos, F. Studer, P. Thevenard, M. Toulemonde, Phys. Rev. **B 51** (1995) 12194.

[16] B. Canut, S.M.M. Ramos, P. Thevenard, N. Moncoffre, A. Benyagoub, G. Marest, A. Meftah, M. Toulemonde, F. Studer, Nucl. Instr. Meth. **B 80-81** (1993) 1114.

[17] K. Schwartz, C. Trautmann, A.S. El-Said, R. Neumann, M. Toulemonde, Phys. Rev. **B 70** (2004) 184104.

[18] A.S. El-Said, R. Neumann, K. Schwartz and C. Trautmann, Nucl. Instr. Meth. **B 245** (2006) 250.

[19] R. Katz, Phys. Rev. **170** (1968) 401

[20] M.P.R Waligorski, R.N. Hamm, R. Katz, Nucl. Tracks Radiat. Meas. **11**, 309 (1986).

[21] A. Meftah, F. Brisard, J.M. Costantini, M. Hag-Ali, J.P. Stoquert, F.Studer, M. Toulemonde, Phys. Rev. **B48** (1993) 920.

[22] A. Dunlop, G. Jaskierowicz, S. Della-Negra, Nucl. Instr. and Meth. **B146** (1998) 302.

[23] A. Adla, V. Buschmann, H. Fuess, C. Trautmann, Nucl. Instr. Meth. **B 185** (2001) 210.

[24] A.S. El-Said, F. Aumayr, S. Della-Negra, R. Neumann, K. Schwartz, M. Toulemonde, C. Trautmann, K.-O. Voss, Nucl. Instr. Meth. **B 256** (2007) 313.

[25] J. Jensen, A. Dunlop, S. Della-Negra, H. Pascard, Nucl. Instr. and Meth. **B135** (1998) 295.

[26] J. Jensen, A. Dunlop, S. Della-Negra, M. Toulemonde, Nucl. Instr. and Meth. **B146** (1998) 412.

[27] M. Toulemonde, G. Fuchs, N. Nguen, F. Studer, D. Groult, Phys. Rev. **B35** (1987) 6560.

[28] P. Hansen and H. Heitmann Phys. Rev. Lett. 43 (1979) 1444.

[29] H. Dammak, A. Dunlop, D. Lesueur, A. Brunelle, S. Della-Negra, Y. Le Beyec, Phys. Rev. Lett. **74** (1995) 1135.

[30] J.F. Ziegler, P. Biersack, U. Littmark, The Stopping and Ranges of Ions in Solids, Pergamon Press, Oxford, 1985.

[31] D. Ben-Hamu, A. Baer, H. Feldman, J. Levin, O. Heber, Z. Vager, D. Zaifman, Phys. Rev. **A 56** (1997) 4786.

[32] C. Tomaschko, D. Brandl, R. Krüger, M. Schurr, H. Voit, Nucl. Instr. Meth. **B 103** (1995) 407.

[33] N. Khalfaoui , C.C. Rotaru, S. Bouffard, M. Toulemonde, J.P. Stoquert , F. Haas, C. Trautmann, J. Jensen, A. Dunlop, Nucl. Instr. Meth. **B 240** (2005) 819.

[34] N. Khalfaoui, PhD Thesis 2003 University of Caen. Web address: **tel-00005926.pdf**

[35] J.M. Costantini, F. Brisard, M. Toulemode, F.Studer, Nucl. Instr. Meth. **B 122** (1997) 514.

[36] Ch. Houpert, F.Studer, D.Groult, M.Toulemonde, Nucl. Instr. Meth. **B 39** (1989) 720.

[37] A. Dunlop, G. Jaskierowicz, J. Jensen, Della-Negra, Nucl. Instr. Meth. **B 132** (1997) 93.

[38] M.Toulemonde, Ch Dufour, A. Meftah, E. Paumier, Nucl. Instr. Meth. **B 166** (2000) 903.

[39] M.Toulemonde, W. Assmann, C. Dufour, A. Meftah, F. Studer, C. Trautmann, Ion Beam Science: Solved and Unsolved Problems, The Royal academy of Science and Letters, Mat. Fys. Medd. 52 (2006) 263.

[40] A. Meftah, M. Djebara, N. Khalfaoui, M. Toulemonde, Nucl. Instr. Meth. **B 146** (1998) 431.

[41] A. Meftah, J.M. Costantini, N. Khalfaoui, Boudjadar, J.P. Stoquert, F. Studer, M. Toulemonde, Nucl. Instr. Meth. **B 237** (2005) 563.

[42] M. Toulemonde, A. Meftah, J.M. Costantini, K. Schwartz, C. Trautmann, Nucl. Instr. and Meth. B 146 (1998) 426.

## FIGURE CAPTIONS

Table 1. Irradiation parameters and correlation coefficients (ρ) for YIG irradiated with $C_{60}$ clusters (this study) together with data from an earlier investigation using monatomic ions [35] and. The energy loss and the projected range were calculated using the SRIM-2006 code [30].

Fig.1. Topographic SFM image of YIG surface irradiated with 30-MeV $C_{60}$ clusters of fluence ~$10^{10}$ $cm^{-2}$.

Fig.2. Frequency distribution of hillocks diameter and height.

Fig.3. Correlation between diameter, and height of hillocks (top) and dependence of correlation coefficient on electronic energy loss (bottom) for YIG irradiated with monatomic [35] and $C_{60}$ cluster ions.

Fig.4. Diameter and height of hillocks as a function of electronic energy loss for monatomic [35] and $C_{60}$ cluster ions.

Fig.5. Hillock height as a function of deposited energy density.

Table 1

| Projectile | Energy (MeV) | velocity ($\beta = v/c$) | $(dE/dx)_e$ (keV/nm) | energy density (eV/atom) | $(dE/dx)_n$ (keV/nm) | projected range (μm) | ρ |
|---|---|---|---|---|---|---|---|
| $^{64}Ni^{(1)}$ | 506 | 0.1303 | 9.8 | 1.7 | 0.01 | 47.3 | - |
| $^{136}Xe^{(1)}$ | 870 | 0.0892 | 27.8 | 2.3 | 0.03 | 36.5 | 0.90 |
| $^{129}Xe^{(1)}$ | 477 | 0.1173 | 28.6 | 3.0 | 0.04 | 23.6 | 0.82 |
| $^{208}Pb^{(1)}$ | 957 | 0.0994 | 40.7 | 3.8 | 0.08 | 31.2 | 0.83 |
| $C_{60}$ | 30 | 0.0094 | 56.3 | 9.6 | 1.50 | 0.7 | 0.74 |

(1) Irradiation at GANIL accelerator.

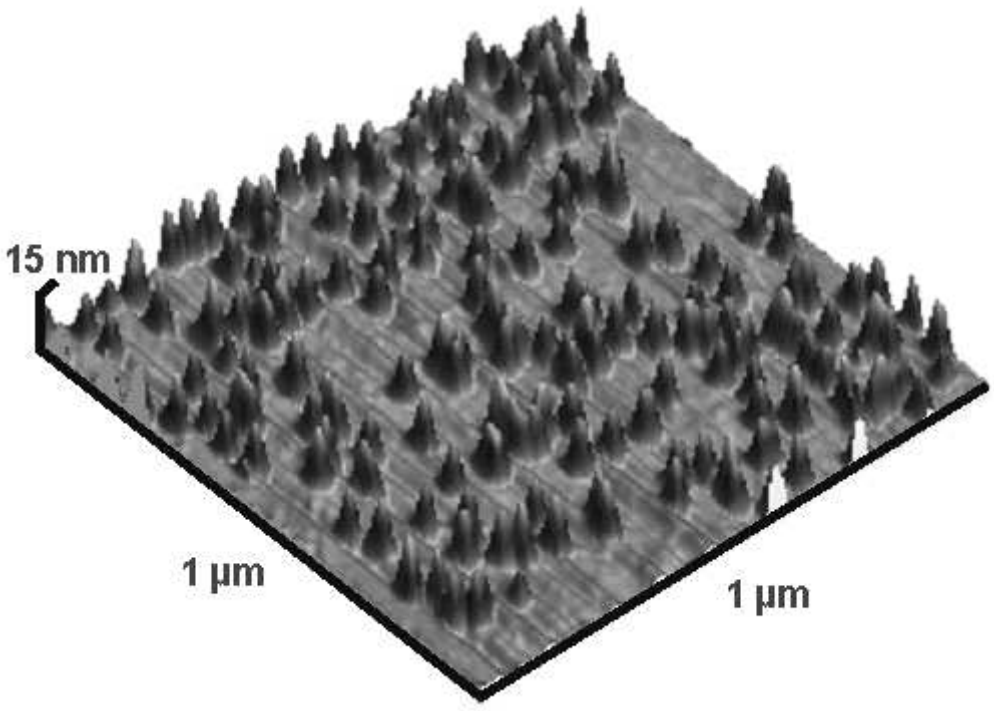


Fig. 1.

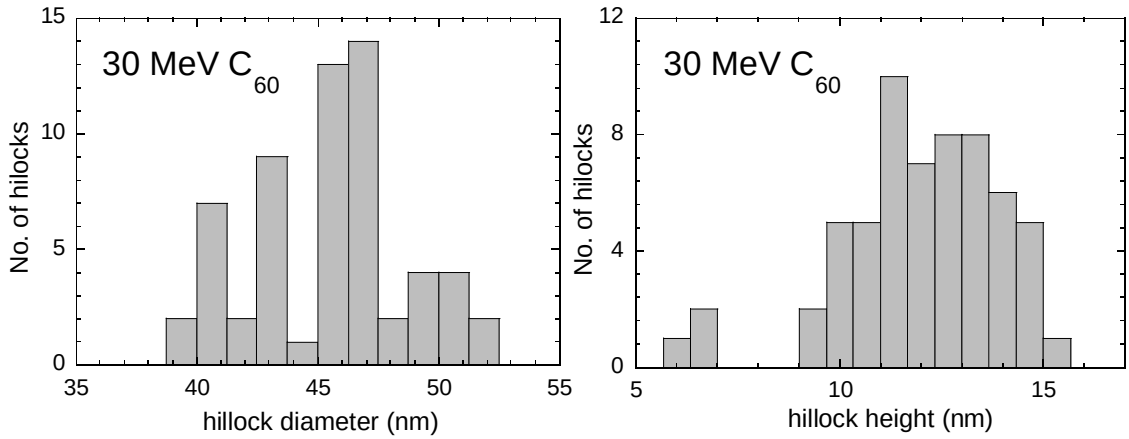
30 MeV C60
No. of hilocks
hillock diameter (nm)
30 MeV C60
No. of hilocks
hillock height (nm)

Fig. 2.

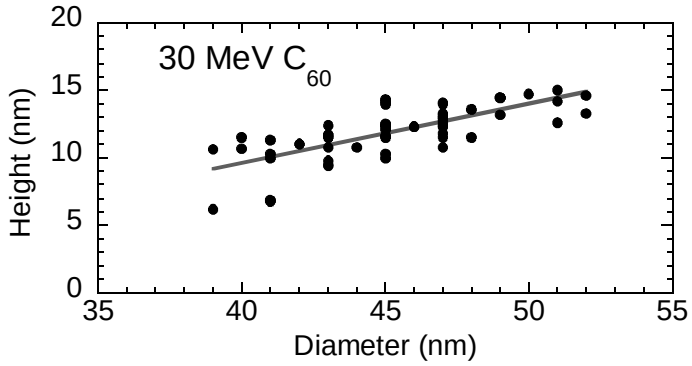
30 MeV C60
Height (nm)
Diameter (nm)

Fig. 3.

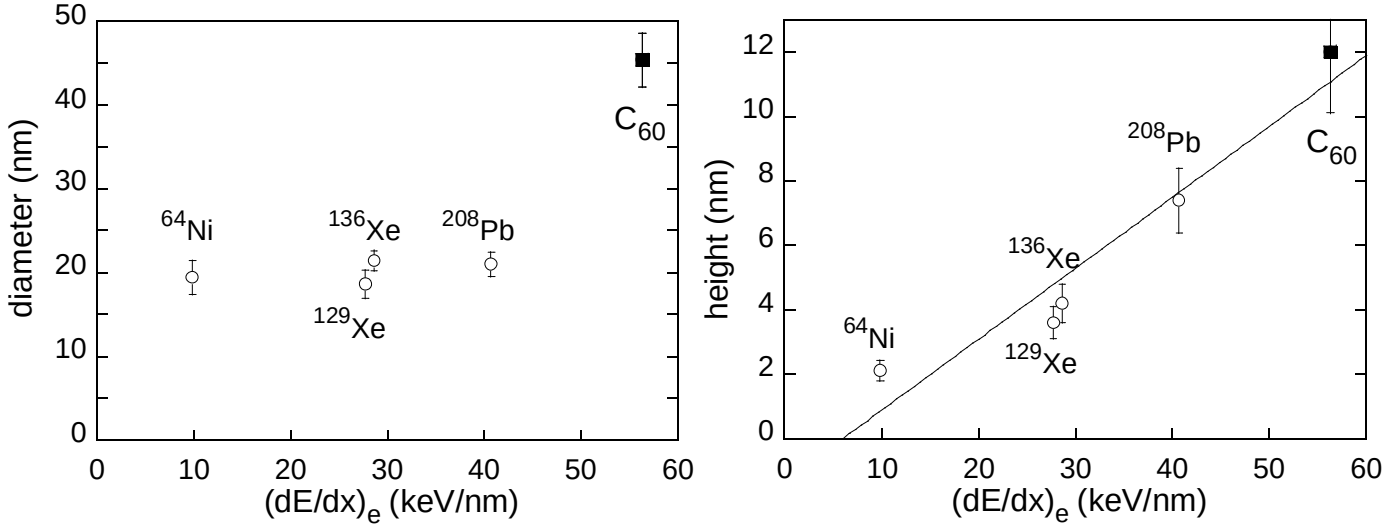
diameter (nm)
(dE/dx)e (keV/nm)
64Ni
136Xe
129Xe
208Pb
C60
height (nm)
(dE/dx)e (keV/nm)
64Ni
136Xe
129Xe
208Pb
C60

Fig. 4.

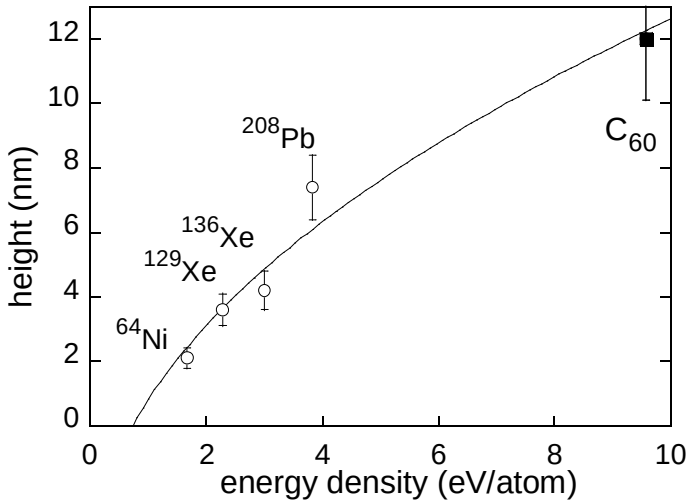
height (nm)
energy density (eV/atom)
64Ni
129Xe
136Xe
208Pb
C60

Fig. 5.